

Superconductivity in FeSe: the role of nematic order

Jian Kang,^{1,*} Rafael M. Fernandes,² and Andrey Chubukov²

¹*National High Magnetic Field Laboratory, Florida State University, Tallahassee, Florida 32304 USA*

²*School of Physics and Astronomy, University of Minnesota, Minneapolis, MN 55455, USA*

Bulk FeSe is a special iron-based material in which superconductivity emerges inside a well-developed nematic phase. We present a microscopic model for this nematic superconducting state, which takes into account the mixing between s -wave and d -wave pairing channels and the changes in the orbital spectral weight promoted by the sign-changing nematic order parameter. We show that nematicity gives rise to a $\cos 2\theta$ variation of the pairing gap on the hole pocket that agrees with ARPES and STM data for experimentally-extracted Fermi surface parameters. We further argue that, in BCS theory, d_{xz} and d_{yz} orbitals give nearly equal contributions to the pairing glue, i.e. nematic order alone accounts for the gap anisotropy, but has little effect on T_c . This result questions the validity of the concept of orbital-selective pairing. Self-energy corrections, however, make d_{xz} orbital more incoherent and reduce its contribution to pairing.

Introduction. Superconductivity in FeSe has attracted a lot of attention recently because this material holds the promise to reveal new physics not seen in other Fe-based superconductors¹. The pairing in FeSe emerges at $T \leq 8$ K from a state with a well-defined nematic order, which develops at a much higher temperature $T_s \sim 90$ K. Because nematic order breaks the C_4 tetragonal symmetry down to C_2 , it mixes the s -wave and d -wave pairing channels^{2–4}. As a result, the pairing gap on the Γ -centered hole pocket, $\Delta(\theta)$, has both s -wave and d -wave components, $\Delta(\theta) = \Delta_1 + \Delta_2 \cos 2\theta$, where Δ_1 and Δ_2 are C_4 -symmetric functions of $\cos 4\theta$. This gap form is generic, but the relative sign between Δ_1 and Δ_2 depends on details of the pairing interaction and the structure of the nematic order.

The $\cos 2\theta$ gap anisotropy on the hole pocket (“ h ” pocket in Fig. 1) has been probed recently by angle resolved photoemission spectroscopy (ARPES)^{5,6} and scanning tunneling microscopy (STM)^{7,8} measurements. These probes have shown^{5,7} that the gap is larger along the direction towards the X electron pocket made out of d_{yz} and d_{xy} orbitals, than towards the Y pocket made out of d_{xz} and d_{xy} orbitals (Fig. 1). The part of the hole pocket where the gap is the largest is predominantly of d_{yz} orbital character. This, combined with indications that the gap on the X pocket is larger in regions where the d_{yz} orbital component is dominant⁷, led to the proposal that the pairing glue in FeSe is orbital-selective and predominantly involves fermions from the d_{yz} orbital.

To support this argument, Refs.^{7,9} analyzed the pairing problem within BCS theory, using the static interaction in the spin channel as the glue. They argued that the experimental gap anisotropy can only be reproduced if one phenomenologically re-calibrates the interactions on d_{xz} , d_{yz} , and d_{xy} orbitals and set the interaction on the d_{yz} orbital to be the strongest. This was done by introducing phenomenologically different frequency and momentum-independent Z -factors for each orbital. A constant Z does not give incoherence, but it does affect the magnitudes of the interactions on different orbitals.

In this paper we reconsider this issue. We argue that one has to distinguish between the difference of the in-

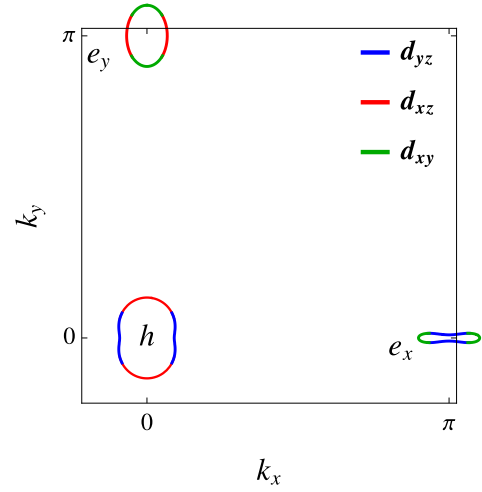


Figure 1. The Fermi surface and its orbital content in the nematic phase of FeSe. In the 1-Fe Brillouin zone there is a hole (h) pocket centered at $\Gamma = (0, 0)$ and two electron pockets X and Y centered at $(\pi, 0)$ and $(0, \pi)$, respectively. STM and ARPES data^{5,7} show that the h pocket is an ellipse elongated along $\Gamma - Y$, and that the X electron pocket has a peanut-type form with the minor axis along the Y direction.

teractions on the d_{xy} orbital and d_{xz}/d_{yz} orbitals, and the difference between the interactions on the d_{xz} and d_{yz} orbitals. The dressed interactions on the d_{xy} orbital and on the d_{xz}/d_{yz} orbitals are not equal already in the tetragonal phase, because they flow to different values as one progressively integrates out contributions from high-energy fermions^{10–12}. Adding different Z -factors to the fermions on d_{xy} and d_{xz}/d_{yz} orbitals is a legitimate way to incorporate these high-energy renormalizations into the low-energy model. On the other hand, the interactions on the d_{xz} and d_{yz} orbitals become different only in the presence of nematic order. Because the latter is experimentally of order 10 meV, which is much smaller than the electronic bandwidth, the splitting of these interactions by high-energy fermions is irrelevant. From

this perspective, the difference between the interactions on d_{xz} and d_{yz} orbitals should be fully captured within the low-energy model, without additional phenomenological $Z_{xz} \neq Z_{yz}$.

In our approach we depart from the tetragonal phase with the Γ -, X -, and Y -centered Fermi pockets in the 1-Fe Brillouin zone. We use the low-energy model of Ref.¹³ to parametrize the dispersion near these three points, and the model of Ref.¹⁰ for the d_{xz}/d_{yz} pairing interactions in the s -wave and d -wave channels. We introduce a two-component d -wave nematic order parameter $\Phi \propto n_{d_{xz}} - n_{d_{yz}} = (\Phi_h, \Phi_e)$, where h and e refer to hole and electron pockets. It reconstructs the dispersion and the Fermi pockets to the ones shown in Fig. 1. The STM results⁷ reveal an ellipsoidal Γ hole pocket elongated along the $\Gamma - Y$ direction, and a peanut-like X electron pocket. A simple analysis shows that such Fermi surfaces emerge if $\Phi_h > 0$ and $\Phi_e < 0$, i.e. the nematic order changes sign between hole and electron pockets. This sign change is consistent with earlier ARPES data^{14,15} and with theoretical analysis^{10,16}. We take as an input the results of earlier studies^{10-12,16-18} that the largest pairing interaction at low-energies is a repulsion between hole and electron pockets. This interaction has s -wave and d -wave components U_s and U_d , respectively. We dress up U_s and U_d by coherence factors associated with the nematic order and write down the gap equation. From its solution we obtain T_c , the sign and magnitude of the $\cos 2\theta$ anisotropy of the superconducting gap on the hole pocket, and the gap anisotropy on the electron pockets.

Our results show that T_c is only moderately affected by nematicity. The pairing in the absence of nematic order yields the standard s^{+-} gap, which changes sign between hole and electron pockets. The key effects of nematicity are the gap anisotropy on the h hole pocket and the non-equivalence of the gaps on the two electron pockets. These results are consistent with two sets of data: (i) the phase diagram of S-doped $\text{FeSe}_{1-x}\text{S}_x$, which shows that T_c changes little between $x < 0.17$, when superconductivity emerges inside a nematic phase, and $x > 0.17$, when there is no nematic order above T_c ; and (ii) thermal conductivity, specific heat, and STM data¹⁹⁻²², which shows that the gap anisotropy changes drastically between $x < 0.17$ and $x > 0.17$.

For the gap on the hole pocket we find $\Delta(\theta_h) \approx \Delta_h(1 + \alpha \cos 2\theta_h + \beta \cos 4\theta_h)$, where the $\cos 2\theta_h$ term is induced by the nematicity and, to leading order in $\Phi_{h,e}$, $\alpha \propto (-4\Phi_e - (U_d/U_s)\Phi_h)$ (see Eq (5) below). In contrast, β exists already in the tetragonal phase, and its value depends on the details of the electronic structure. Because $\Phi_h > 0$ and $\Phi_e < 0$, the two terms in α have opposite signs. The experimental angular dependence of the gap is reproduced when the Φ_e term is larger. We computed the dimensionless $\Phi_{h,e}$ using band structure parameters that fit the ARPES and STM data²³ and found $2|\Phi_e| \sim \Phi_h \sim 0.2$. Combining this with the fact that $U_s \geq U_d$ (see below), we see that α is positive. A

positive α can be interpreted as if nematicity makes the pairing interaction between the Γ and X pockets stronger than between the Γ and Y pockets. We emphasize that this effect is fully captured within the low-energy model.

In Fig. 2 we show the calculated $\Delta(\theta_h)$ along with the gap anisotropy extracted from the STM data^{7,24}. We see that the agreement is quite good.

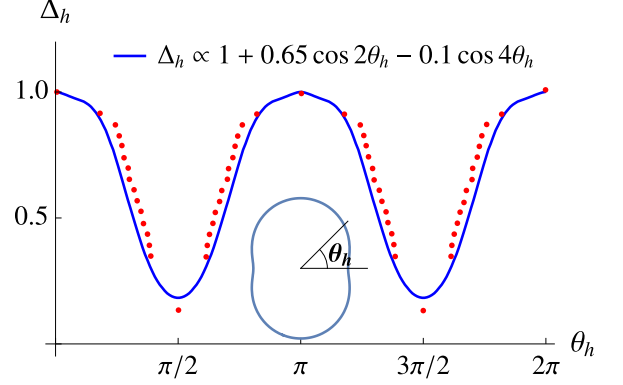


Figure 2. Angular dependence of the pairing gap on the hole pocket obtained by numerically solving the gap equations with band structure parameters and nematic order parameters fitted to ARPES data above T_c . The gap maximum is along the $\Gamma - X$ direction, consistent with STM and ARPES data^{7,24}. Points are STM data from Ref.⁷. The gap function $\Delta(\theta_h) = \Delta_h(1 + \alpha \cos 2\theta_h + \beta \cos 4\theta_h)$ has the $\cos 2\theta$ terms induced by nematicity (which we explicitly computed), as well as C_4 -symmetric anisotropic $\cos 4\theta$ terms present already in the tetragonal phase due to spin-orbit coupling¹³ and/or due to dressing of the pairing interaction by high-energy fermions^{10,17}.

We also go beyond mean-field and analyze the nematicity-induced fermionic self-energy. We argue that there are two competing effects. On one hand, nematic order makes the interaction on the Y pocket weaker than on the X pocket, and this tends to increase the quasi-particle residue on the Y pocket compared to that on the X pocket. On the other hand, nematic order increases the portion of the Y pocket where excitations have predominantly d_{xy} orbital character, and makes the d_{xy} -dominated portion smaller on the X pocket (see Fig. 3). If the d_{xy} excitations are not observed because of matrix elements, or if the d_{xy} orbital is more incoherent than the d_{xz}/d_{yz} orbitals, as some studies suggested²⁵⁻²⁸, the Y pocket may actually become less visible in ARPES and STM, as these experiments seem to suggest^{7,14,29}.

Low-energy model. We consider a quasi-2D model of bulk FeSe, which in the tetragonal phase has two hole pockets centered at the Γ point and two electron pockets centered at the X and Y points of Fe-only Brillouin zone. The hole pockets are made out primarily of d_{xz} and d_{yz} orbitals, the X pocket is made primarily out of d_{yz} and d_{xy} orbitals, and the Y pocket, of d_{xz} and d_{xy} orbitals. We model the low-energy electronic structure on each pocket by spinors, following Ref.^{13,30}. We

choose parameters such that the larger hole pocket h has d_{xz} character along the $\Gamma - Y$ direction and d_{yz} character along the $\Gamma - X$ direction, consistent with ARPES experiments¹⁴.

The band operators for h , X , and Y pockets are expressed in terms of the orbital operators as

$$\begin{aligned} h &= d_{yz} \cos \phi_h + d_{xz} \sin \phi_h \\ e_X &= -id_{yz} \cos \phi_X + d_{xy} \sin \phi_X \\ e_Y &= id_{xz} \cos \phi_Y + d_{xy} \sin \phi_Y, \end{aligned} \quad (1)$$

In the tetragonal phase, the h -pocket is nearly circular and $\phi_h \approx \theta_h$, where θ_h is the angle measured with respect to the $\Gamma - X$ axis. On electron pockets, to a good approximation $\cos \phi_{X,Y} = A \sin \theta_{X,Y}$, $\sin \phi_{X,Y} = (1 - A^2 \sin^2 \theta_{X,Y})^{1/2}$, where $A < 1$ and θ_X (θ_Y) is the angle measured with respect to the $\Gamma - X$ ($\Gamma - Y$) direction^{3,11}.

In the nematic phase we introduce momentum-dependent d -wave nematic order $\Phi(k) \propto n_{xz} - n_{yz}$ with components $\Phi(\Gamma) = \Phi_h$ and $\Phi(X) = -\Phi(Y) = \Phi_e$. For simplicity, we neglect the d_{xy} component of the nematic order^{11,31}. Eqs. (1) still hold in the presence of nematicity, but the relations between ϕ_h, ϕ_X, ϕ_Y and the angles along the Fermi surfaces become different and are obtained by the diagonalization of the corresponding quadratic Hamiltonians. For the hole pocket, we define dimensionless Φ_h via $\cot 2\phi_h = \cot 2\theta_h - 2\Phi_h / \sin 2\theta_h$ (Ref.²³). To first order in Φ_h , $\phi_h = \theta_h + \Phi_h \sin 2\theta_h$. The sign of Φ_h must be positive to match STM and ARPES data^{6,7,14,15}, which all show that the h pocket is elongated in the $\Gamma - Y$ direction. The second hole pocket sinks below the Fermi level at $T \leq T_s$ and we will not include it into our model. For electron pockets we find that the relations $\cos \phi_{X,Y} = A \sin \theta_{X,Y}$ also hold, but A becomes different for X and Y pockets. We define dimensionless Φ_e via $A_X \approx A(1 - \Phi_e)$ and $A_Y \approx A(1 + \Phi_e)$, up to $O(\Phi_e^2)$ terms. The sign of Φ_e must be negative to reproduce STM and ARPES results^{7,15} that the X pocket has a peanut-like shape with the minor axis at $\theta_X = \pm\pi/2$. A negative Φ_e increases the weight of d_{yz} orbital on the X pocket and reduces the weight of d_{xz} orbital on the Y pocket, as shown in Fig. 3. The positive Φ_h also increases the d_{xz} spectral weight on the hole pocket.

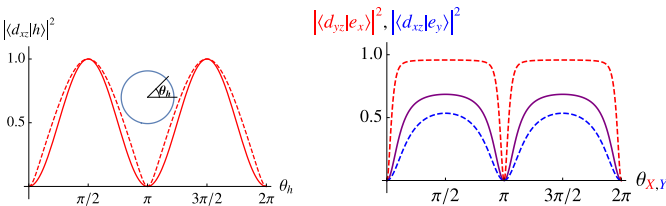


Figure 3. The change of orbital weight on the hole pockets (left panel) and on the electron pocket (right panel) between the tetragonal phase (solid line) and the nematic phase (dashed lines). The angle θ_X (θ_Y) is measured with respect to the $\Gamma - X$ ($\Gamma - Y$) direction.

Pairing interaction. The pairing interaction has three components – one involves fermions near the hole pocket, another involves fermions near the two electron pockets, and the third one is the pair hopping between hole and electron pockets. At the bare level all three interactions are comparable, but earlier studies have found^{7,10–12,17} that the pair-hopping term gets enhanced once one integrates out fermions with high energies. This enhancement can be understood as an indication of the system’s tendency to increase magnetic fluctuations at momenta connecting the Γ and the X/Y points, consistent with the neutron scattering data^{32–34}. We therefore consider only the pair hopping term for the pairing problem. In the band basis, the pair-hopping pairing interaction has the form

$$\begin{aligned} H_{\text{pair}} &= h_k^\dagger h_{-k}^\dagger [U_s (e_{X,p} e_{X,-p} \cos^2 \phi_X + e_{Y,p} e_{Y,-p} \cos^2 \phi_Y) \\ &\quad + U_d \cos 2\phi_h (e_{X,p} e_{X,-p} \cos^2 \phi_X - e_{Y,p} e_{Y,-p} \cos^2 \phi_Y)] \end{aligned} \quad (2)$$

where repeated momentum indices are implicitly summed and spin indices are omitted. In the tetragonal phase, $\cos^2 \phi_{X,Y} = A^2(1 - \cos 2\theta_{X,Y})/2$, $\phi_h = \theta_h$, and the two terms in (2) describe pairing interactions in the s -wave and d -wave channels with couplings U_s and U_d , respectively. The ratio U_s/U_d is close to 1 at the bare level, but increases under RG¹⁰, such that the leading instability in the absence of nematicity is towards s^{+-} superconductivity.

In the presence of nematic order the situation changes because now $\cos 2\phi_h \approx \cos 2\theta_h - \Phi_h$ and $A_X \neq A_Y$. As a result, the U_d term in (2) acquires extra terms which have an “ s -wave” angular dependence and effectively renormalize the U_s term, making this interaction different for fermions near the X and Y pockets. Substituting the forms of $\cos 2\phi_h, \cos 2\phi_X$ and $\cos 2\phi_Y$ into (2) and restricting to first-order terms in Φ_h and Φ_e , we obtain the pairing interaction in the form

$$H_{\text{pair}} = \frac{A^2}{2} \sum_{j=X,Y} h_k^\dagger h_{-k}^\dagger (A_j + B_j \cos 2\theta_h) e_{j,p} e_{j,-p} \quad (3)$$

where

$$\begin{aligned} A_{X,Y} &= (1 - \cos 2\theta_{X,Y}) [U_s (1 \mp 2\Phi_e) \mp U_d \Phi_h] \\ B_{X,Y} &= \pm U_d (1 - \cos 2\theta_{X,Y}) (1 \mp 2\Phi_e) \end{aligned} \quad (4)$$

Gap equations. We use Eqs. (3) and (4) to write the linearized gap equations. The gap on the hole pocket is parametrized by $\Delta(\theta_h) = \Delta_h(1 + \alpha \cos 2\theta_h)$, where the gap anisotropy α is induced by nematicity (we neglected $\cos 4\theta$ term to simplify presentation). The computational steps are rather conventional and are presented in²³. The result, to linear order in $\Phi_{e,h}$, is:

$$\alpha \approx -\frac{U_s U_d}{U_s^2 - U_d^2/2} \left(4\Phi_e + \frac{U_d}{U_s} \Phi_h \right) \quad (5)$$

Notice that α depends only on the ratio U_d/U_s , and not on the strength of the interaction, which is compensated by the Cooper logarithm.

We see that there are two contributions to the gap anisotropy α , originating from the components of the nematic order on hole and electron pockets. Because Φ_h and Φ_e have opposite signs, the sign of α depends on their strength and on the ratio between the interactions U_d/U_s . We computed the dimensionless $\Phi_{h,e}$ using band structure parameters that fit the ARPES data for the dispersion^{35,36} and STM data⁷ for the shapes of the FSs in the nematic phase above T_c and obtained $2|\Phi_e| \sim \Phi_h \sim 0.2$ (see²³ for details). The same fit yields nematicity-induced splittings between the energies of d_{xz} and d_{yz} orbitals at Γ and X/Y at around 20 meV, consistent with ARPES data^{35,37}. The bare values of U_s and U_d are quite similar, $U_s = U + J$ and $U_d = U - J$, where U and J are Hubbard and Hund's interactions. Then $4\Phi_e \approx -2\Phi_h(U_d/U_s)$, i.e., $\alpha \sim 0.4$ is positive, and the gap $\Delta_h(\theta_h)$ has its maximum along the $\Gamma - X$ direction $\theta_h = 0$. This is consistent with the STM and ARPES data^{7,24}. The Φ_h term in (5) is further reduced if we take into account the fact that the ratio U_s/U_d grows under the renormalization group flow¹⁰.

To go beyond this analytic expansion in powers of $\Phi_{e,h}$, we solved the gap equations numerically for the same set of parameters, but not restricting to first order in $\Phi_{h,e}$ (see²³). We found the same gap structure but somewhat larger α (≈ 0.65 instead of ≈ 0.4). The result is shown in Fig. 2 along with the STM data from Ref.⁷. For this plot, we added to $\Delta(\theta_h)$ additional $\beta \cos 4\theta_h$ term with $\beta = -0.1$ ²³. The $\cos 4\theta_h$ dependence arises already in the tetragonal phase and is determined by details beyond our model.

The sign of the gap anisotropy can be interpreted as the indication that in the nematic state the pairing interaction between h and X pockets becomes stronger than between h and Y pockets. Furthermore, because the positive contribution to α comes from Φ_e , the relative increase of $h - X$ interaction can be traced back to the increase of the spectral weight of d_{yz} orbital on the X pocket. In this respect, qualitatively, our results agree with Refs.^{7,9}, where the increase of the spectral weight on d_{yz} orbital was introduced phenomenologically, via orbital dependent Z -factor. We emphasize, however, that in our theory the modification of d_{xz}/d_{yz} orbital weight naturally emerges in the analysis within the low-energy model and does not require the inclusion of additional Z -factors.

On the electron pockets, to leading order in $\Phi_{h,e}$, the gaps have the forms $\Delta_{X,Y} = -\Delta_h \gamma_{X,Y} (1 - \cos 2\theta_{X,Y})$, where $\gamma_{X,Y} = \gamma [1 \mp (2\Phi_e + U_d/U_s \Phi_h - \alpha/2)]$ and $\gamma > 0$ is the number whose value depends on the electronic structure. The vanishing of the gaps at $\cos 2\theta_{X,Y} = \pm 1$ is an artefact of neglecting the d_{xy} orbital in the pairing problem. As we said, the pairing interaction involving d_{xy} fermions gets reduced in the RG flow, but is still non-zero. Consequently, the gaps $\Delta_{X,Y}$ tend to small

but finite values along the $\Gamma - X$ and $\Gamma - Y$ directions, respectively. The STM data⁷ reported an anisotropic, but still sign-preserving gap on the X pocket, with gap maximum at $\theta_X = \pi/2$, consistent with our formulas. The overall sign of $\Delta_{X,Y}$ is opposite to that of Δ_h . The dependence of $\gamma_{X,Y}$ on the nematic order shows that the gap magnitude is larger on the X pocket than on the Y pocket. We propose to verify this in future experiments.

Fermionic self-energy. The STM data indicate that in the nematic phase the Y pocket is less visible than the X pocket, and in some ARPES studies²⁹ this Y pocket has not been observed. To understand this feature, we computed the self-energy on both electron pockets to second order in U_s and U_d and extracted the actual quasiparticle residues $Z_{X,Y}$ on each electron pocket²³. We find $Z_Y > Z_X$ simply because the effective interaction is larger for fermions on the X pocket (we recall that larger interaction is translated as a smaller Z). If this was the only effect, we would expect the Y pocket to become more visible. However, like we said, the nematicity also decreases the d_{xz} orbital spectral weight of the Y pocket and increases the d_{yz} spectral weight of the X pocket (see Fig. 3). Thus, nematicity increases d_{xy} content on the Y pocket and reduces it on the X pocket. If the d_{xy} orbital excitations are not observed in STM and ARPES because of matrix elements, or if the d_{xy} orbital is more incoherent than the d_{xz}/d_{yz} orbitals²⁵⁻²⁸, then the Y pocket should indeed become less visible in the nematic phase. We also note that nematicity-induced $Z_{X,Y}$ scales as $U_{s,d}/W$, where W is of the order of the bandwidth. This dependence is subleading to the one which determines α , at least at weak coupling. As a consequence, inserting the self-energy into the gap equation only leads to a small correction to α . The situation may be different at strong coupling.

Conclusions. In this paper we argued that the experimentally observed anisotropy of the superconducting gap in bulk FeSe can be explained within the low-energy model for nematic order, without adding phenomenologically different quasiparticle weights for the d_{xz}/d_{yz} orbitals. Our key result is that T_c is not strongly affected by nematic order, but nematicity mixes s -wave and d -wave pairing channels and gives rise to a $\cos 2\theta_h$ gap anisotropy on the hole pocket, bringing the minimum of the gap to a smaller value. The sign of the $\cos 2\theta_h$ term is determined by the interplay between the nematic order parameters on hole and electron pockets, which are of different sign, and the relative strength of s -wave and d -wave components of the pairing interaction. When the s -wave component is larger, the hole gap maximum is in the $\Gamma - X$ direction, in agreement with the data. On the peanut-like X pocket, the gap is found to be maximum along the minor axis, which is also in agreement with the data. We also argued that nematicity decreases the weight of the d_{xy} orbital on the X pocket and increases it on the Y pocket. This may explain why the Y pocket is less visible in STM and in some ARPES data.

ACKNOWLEDGMENTS

We are thankful to B. Andersen, S. Borisenko, A. Coldea, P. Hirschfeld, A. Kreisel, C. Meingast, J.C. Séamus Davis, O. Vafek, M. Watson, and Y. Y. Zhao for useful discussions. JK was supported by the National High Magnetic Field Laboratory through NSF Grant No. DMR-1157490 and the State of Florida.

RMF and AVC were supported by the Office of Basic Energy Sciences, U.S. Department of Energy, under awards DE-SC0012336 (RMF) and DE-SC0014402 (AVC). J.K. thanks FTPI at the University of Minnesota for hospitality during the completion of this work. The authors are thankful to KITP at UCSB, where part of the work has been done. KITP is supported by NSF grant PHY 17-48958.

-
- * jian.kang@fsu.edu
- ¹ see e.g., Anna E. Böhrer, Andreas Kreisel, *Journal of Physics: Condensed Matter* **30**, 023001 (2017) and references therein.
 - ² R. M. Fernandes, and A. J. Millis, *Phys. Rev. Lett.* **111**, 127001 (2013);
 - ³ J. Kang, A. F. Kemper, and R. M. Fernandes, *Phys. Rev. Lett.* **113**, 217001 (2014).
 - ⁴ G. Livanas, A. Aperis, P. Kotetes, and G. Varelogiannis, *Phys. Rev. B* **91**, 104502 (2015).
 - ⁵ H. C. Xu, X. Niu, D. F. Xu, J. Jiang, Q. Yao, Q. Y. Chen, Q. Song, M. Abdel-Hafiez, D. A. Chareev, A. N. Vasiliev, Q. S. Wang, H. L. Wo, J. Zhao, R. Peng, and D. L. Feng, *Phys. Rev. Lett.* **117**, 157003 (2016).
 - ⁶ T. Hashimoto, Y. Ota, H. Q. Yamamoto, Y. Suzuki, T. Shimojima, S. Watanabe, C. Chen, S. Kasahara, Y. Matsuda, T. Shibauchi, K. Okazaki, and S. Shin, *Nat. Comm.* **9**, 282 (2018).
 - ⁷ P. O. Sprau, A. Kostin, A. Kreisel, A. E. Böhrer, V. Taufour, P. C. Canfield, S. Mukherjee, P. J. Hirschfeld, B. M. Andersen, and J. C. Séamus Davis, *Science* **357**, 6346 (2017).
 - ⁸ L. Jiao, C.-L. Huang, S. Rößler, C. Koz, U. K. Rößler, U. Schwarz, and S. Wirth, *Scientific Reports*, **7**, 44024 (2017).
 - ⁹ A. Kreisel, B. M. Andersen, P. O. Sprau, A. Kostin, J.C. Séamus Davis, P. J. Hirschfeld, *Phys. Rev. B* **95**, 174504 (2017).
 - ¹⁰ A. V. Chubukov, M. Khodas, R. M. Fernandes, *Phys. Rev. X* **6**, 041045 (2016).
 - ¹¹ R.-Q. Xing, L. Classen, M. Khodas, A. V. Chubukov, *Phys. Rev. B* **95**, 085108 (2017); L. Classen, R.-Q. Xing, M. Khodas, A. V. Chubukov, *Phys. Rev. Lett.* **118**, 037001 (2017).
 - ¹² Fa Wang, Hui Zhai, Ying Ran, Ashvin Vishwanath, Dung-Hai Lee, *Physical Review Letters*, **102**, 047005 (2009); Christian Platt, Werner Hanke, Ronny Thomale, *Advances in Physics* **62**, 453-562 (2013).
 - ¹³ V. Cvetkovic and O. Vafek, *Phys. Rev. B* **88**, 134510 (2013).
 - ¹⁴ A. I. Coldea and M. D. Watson, arXiv:1706.00338.
 - ¹⁵ Y. Suzuki, T. Shimojima, T. Sonobe, A. Nakamura, M. Sakano, H. Tsuji, J. Omachi, K. Yoshioka, M. Kuwata-Gonokami, T. Watashige, R. Kobayashi, S. Kasahara, T. Shibauchi, Y. Matsuda, Y. Yamakawa, H. Kontani, and K. Ishizaka, *Phys. Rev. B* **92**, 205117 (2015).
 - ¹⁶ S. Onari, Y. Yamakawa, and H. Kontani, *Phys. Rev. Lett.* **116**, 227001 (2016).
 - ¹⁷ S. Graser, T. A. Maier, P. J. Hirschfeld, and D. J. Scalapino, *New J. Phys.* **11**, 025016 (2009).
 - ¹⁸ A.V. Chubukov, *Annul. Rev. Cond. Mat. Phys.* **3**, 13.1 (2012).
 - ¹⁹ P. Bourgeois-Hope, S. Chi, D. A. Bonn, R. Liang, W. N. Hardy, T. Wolf, C. Meingast, N. Doiron-Leyraud, and L. Taillefer, *Phys. Rev. Lett.* **117**, 097003 (2016).
 - ²⁰ L. Wang, F. Hardy, T. Wolf, P. Adelman, R. Fromknecht, P. Schweiss, C. Meingast, *Phys. Status Solidi B* **254**, 1600153 (2017).
 - ²¹ Y. Sato, S. Kasahara, T. Taniguchi, X.Z. Xing, Y. Kasahara, Y. Tokiwa, T. Shibauchi, and Y. Matsuda, arXiv:1705.09074.
 - ²² T. Hanaguri, K. Iwaya, Y. Kohsaka, T. Machida, T. Watashige, S. Kasahara, T. Shibauchi, and Y. Matsuda, arXiv:1710.02276.
 - ²³ see Supplementary Material.
 - ²⁴ A very similar gap structure has been extracted from ARPES data, X.J. Zhou et al, private communication.
 - ²⁵ N. Lanata, H. U. R. Strand, G. Giovannetti, B. Hellsing, L. de Medici, and M. Capone, *Phys. Rev. B* **87**, 045122 (2013).
 - ²⁶ Z. P. Yin, K. Haule, and G. Kotliar, *Nat. Mater.* **10**, 932 (2011).
 - ²⁷ E. Bascones, B. Valenzuela, and M. J. Calderón, *Phys. Rev. B* **86**, 174508 (2012).
 - ²⁸ L. Fanfarillo, G. Giovannetti, M. Capone, and E. Bascones, *Phys. Rev. B* **95**, 144511 (2017).
 - ²⁹ M. D. Watson, A. A. Haghighirad, L. C. Rhodes, M. Hoesch, T. K. Kim, *New J. Phys.* **19**, 103021 (2017).
 - ³⁰ R. M. Fernandes and A. V. Chubukov, *Rep. Prog. Phys.* **80**, 014503 (2017).
 - ³¹ R. M. Fernandes and O. Vafek, *Phys. Rev. B* **90**, 214514 (2014).
 - ³² M. C. Rahn, R. A. Ewings, S. J. Sedlmaier, S. J. Clarke, and A. T. Boothroyd, *Phys. Rev. B* **91**, 180501 (2015).
 - ³³ Q. Wang, Y. Shen, B. Pan, Y. Hao, M. Ma, F. Zhou, P. Steffens, K. Schmalzl, T. R. Forrest, M. Abdel-Hafiez, X. Chen, D. A. Chareev, A. N. Vasiliev, P. Bourges, Y. Sidis, H. Cao, and J. Zhao, *Nat. Mater.* **15**, 159 (2016).
 - ³⁴ Q. Wang, Y. Shen, B. Pan, X. Zhang, K. Ikeuchi, K. Iida, A. D. Christianson, H. C. Walker, D. T. Adroja, M. Abdel-Hafiez, X. Chen, D. A. Chareev, A. N. Vasiliev, and J. Zhao, *Nat. Comm.* **7**, 12182 (2016).
 - ³⁵ M. D. Watson, T. K. Kim, L. C. Rhodes, M. Eschrig, M. Hoesch, A. A. Haghighirad, and A. I. Coldea, *Phys. Rev. B* **94**, 201107 (2016).
 - ³⁶ A. I. Coldea, private communication.
 - ³⁷ A. Fedorov, A. Yaresko, T. K. Kim, Y. Kushnirenko, E. Haubold, T. Wolf, M. Hoesch, A. Grüneis, B. Büchner, and S. V. Borisenko, *Scientific Reports*, **6**, 36834 (2016).

Supplementary material for “Anisotropic superconductivity in FeSe without orbital selectivity”

I. DETAILS OF THE LOW-ENERGY MODEL

A. Hole Pockets

The dispersion near the hole pockets centered at Γ is expressed in terms of the two-component spinor $\psi_\Gamma = (d_{xz}, d_{yz})^T$. Following Refs.^{13,30}, the Hamiltonian in the tetragonal phase is

$$H_\Gamma^{(0)} = \psi_\Gamma^\dagger \left(\left(\epsilon_\Gamma - \frac{k^2}{2m_\Gamma} \right) \tau_0 - \frac{b}{2} (k_x^2 - k_y^2) \tau_3 - 2ck_x k_y \tau_1 \right) \psi_\Gamma = \psi_\Gamma^\dagger (H_0 \tau_0 - \frac{b}{2} k^2 \cos 2\theta_h \tau_3 - ck^2 \sin 2\theta_h \tau_1) \psi_\Gamma, \quad (\text{S1})$$

where θ_h is the angle measured with respect to the $\Gamma - X$ axis (note that we work in the 1-Fe Brillouin zone). The free parameters of this Hamiltonian are shown in Table S1, and are obtained from fitting to ARPES data^{35,36}. All the energy parameters are in units of meV, and the momentum are in units of the inverse lattice constant.

ϵ_Γ	$(2m_\Gamma)^{-1}$	b	c
13.6	-473	529	-265

Table S1. Band parameters of the hole pocket.

Besides the numerical solution, it is interesting and sometimes convenient to obtain an approximate analytical solution for the gap equations. For this purpose, note that the ARPES fitted parameters give $b \approx -2c > 0$, therefore, the band dispersion around Γ can be approximated as

$$H_\Gamma^{(0)} \approx H_0(k) \tau_0 + H_1(k) (-\cos 2\theta_h \tau_3 + \sin 2\theta_h \tau_1) \quad (\text{S2})$$

with $H_0 = \epsilon_\Gamma - k^2/(2m_\Gamma)$ and $H_1(\mathbf{k}) \approx bk^2/2$. Diagonalization leads to Eq. (1) of the main text with $\varphi_h = \theta_h$ and an isotropic dispersion, $\epsilon_h = \epsilon_\Gamma + k^2/(2m_\Gamma) + bk^2/2$.

In the nematic phase, the Hamiltonian acquires the extra term $H_\Gamma^{(\text{nem})} = \Delta_h^{(\text{nem})} \psi_\Gamma^\dagger \tau_3 \psi_\Gamma$ (see Ref.³¹). The total Hamiltonian $H_\Gamma = H_\Gamma^{(0)} + H_\Gamma^{(\text{nem})}$ is then:

$$H_\Gamma \approx H_0(k) \tau_0 + \left((\Delta_h^{(\text{nem})} - H_1 \cos 2\theta_h) \tau_3 + H_1 \sin 2\theta_h \tau_1 \right) \longrightarrow H_0(k) \tau_0 + H'_1 (-\cos 2\varphi_h \tau_3 + \sin 2\varphi_h \tau_1) \quad (\text{S3})$$

with:

$$\cot 2\varphi_h \approx \frac{H_1 \cos 2\theta_h - \Delta_h^{(\text{nem})}}{H_1 \sin 2\theta_h} = \cot 2\theta_h - \frac{\Delta_h^{(\text{nem})}}{H_1 \sin 2\theta_h} \implies \varphi_h \approx \theta_h + \Phi_h \sin 2\theta_h \quad (\text{S4})$$

where we defined the dimensionless nematic order parameter $\Phi_h \equiv \Delta_h^{(\text{nem})}/2H_1(k_F)$. Note that $H_1(k_F)$, computed at the Fermi level, gives the splitting between the two hole pockets in the tetragonal phase. Based on the ARPES measurements^{35,37}, we estimate $2H_1(k_F) \approx 50$ meV and $\Delta_h^{(\text{nem})} = 10$ meV, leading to $\Phi_h \approx 0.2$.

In addition to the change in the orbital composition of the Γ pocket, nematicity also deforms the shape of Fermi surface. The change in the dispersion is $\delta\epsilon_h = -\Delta_h^{(\text{nem})} \cos 2\theta_h$, giving rise to a change in the Fermi momentum $\delta k_f \sim -\Delta_h^{(\text{nem})} \cos 2\theta_h / v_f$. Consequently, the Fermi pocket changes shape from circular to elliptical. When $\Delta_h^{(\text{nem})}$ is positive, its major axis points along $\Gamma - Y$, while the minor axis points along $\Gamma - X$.

B. Electron Pockets

For the electron pockets, an analytic expression similar to the case of the hole pocket is not available. We start from the Hamiltonian^{13,30},

$$H_{X,Y} = \Psi_{X,Y}^\dagger \begin{pmatrix} \epsilon_1 + \frac{k^2}{2m_1} \mp \frac{a_1}{2} (k_x^2 - k_y^2) & -iv_{X,Y}(\mathbf{k}) \\ iv_{X,Y}(\mathbf{k}) & \epsilon_3 + \frac{k^2}{2m_3} \mp \frac{a_3}{2} (k_x^2 - k_y^2) \end{pmatrix} \Psi_{X,Y} \quad (\text{S5})$$

$$v_X(\mathbf{k}) = \sqrt{2}v_{k_y} + \frac{p_1}{\sqrt{2}}(k_y^3 + 3k_y k_x^2) - \frac{p_2}{\sqrt{2}}k_y(k_x^2 - k_y^2), \quad v_Y(\mathbf{k}) = \sqrt{2}v_{k_x} + \frac{p_1}{\sqrt{2}}(k_x^3 + 3k_x k_y^2) + \frac{p_2}{\sqrt{2}}k_x(k_x^2 - k_y^2)$$

Here we list the band parameters fitted to ARPES experiments^{35,36}. All the energy parameters are in units of meV, and the momenta are in units of the inverse lattice constant.

ϵ_1	ϵ_3	$(2m_1)^{-1}$	$(2m_3)^{-1}$	a_1	a_3	v	p_1	p_2
-19.9	-39.4	1.4	186	136	-403	-122	-137	-11.7

Table S2. Band parameters for the electron pockets.

Upon numerically diagonalizing the Hamiltonian, we found that the orbital composition of the X electron pocket can be fitted using the approximate form for the band operator in terms of the orbital operators:

$$e_X = -iA \sin \theta_X d_{yz} + \sqrt{1 - A^2 \sin^2 \theta_X} d_{xy} \quad (S6)$$

The value of A can be estimated using the band parameters presented below, yielding $A^2 \approx 0.7$. Note that there is another band at the X pocket that does not cross the Fermi level. The corresponding operator, denoted here by \tilde{e}_X , is parametrized according to:

$$\tilde{e}_X = i\sqrt{1 - A^2 \sin^2 \theta_X} d_{yz} + A \sin \theta_X d_{xy} \quad (S7)$$

An important quantity for our analysis is the energy splitting ΔE between these two bands calculated at k_F of the electron pocket. Using the ARPES fitted parameters, we find $\Delta E \sim 60\text{meV}$ for $\theta = \pi/2$.

Nematic order is included via:

$$H_{X,Y}^{(\text{nem})} = \mp \Delta_e^{(\text{nem})} \Psi_{X,Y}^\dagger \begin{pmatrix} 1 & 0 \\ 0 & 0 \end{pmatrix} \Psi_{X,Y} . \quad (S8)$$

To leading order of $\Delta_e^{(\text{nem})}$, the wave function of the upper band becomes

$$e'_X \approx e_X + \frac{\Delta_e^{(\text{nem})}}{\Delta E} A \sin \theta_X \sqrt{1 - A^2 \sin^2 \theta_X} \left(i\sqrt{1 - A^2 \sin^2 \theta_X} d_{yz} + A \sin \theta_X d_{xy} \right) \quad (S9)$$

At $\theta_X = \pi/2$, where the spectral weight of d_{yz} orbital is maximum, we find that e'_X can be expressed in the same form of e_X but with $A \rightarrow A_X = A + \delta A$, where:

$$\frac{\delta A}{A} \approx -\frac{\Delta_e^{(\text{nem})}}{\Delta E} (1 - A^2) \equiv -\Phi_e \quad (S10)$$

Here, we defined the dimensionless nematic order parameter Φ_e . Using the values of A and ΔE mentioned above, and $\Delta_e^{(\text{nem})} \approx -18\text{meV}$, as indicated by ARPES measurements^{14,37}, we find $\Phi_e \approx -0.1$.

II. PAIRING INTERACTION

As explained in the main text, the RG analysis allows us to focus only on two types of inter-pocket pairing interaction: the intra-orbital pairing U and inter-orbital pairing J . We find

$$H_{\text{pair}}^{(X)} = 2 \sum_{\mathbf{k}, \mathbf{p}} h_{\mathbf{k}\uparrow}^\dagger h_{-\mathbf{k}\downarrow} (1 - t \cos 4\phi_h) (U \cos^2 \phi_h + J \sin^2 \phi_h) e_{X-\mathbf{p}\downarrow} e_{X\mathbf{p}\downarrow} \cos^2 \phi_X + h.c. \quad (S11)$$

$$H_{\text{pair}}^{(Y)} = 2 \sum_{\mathbf{k}, \mathbf{p}} h_{\mathbf{k}\uparrow}^\dagger h_{-\mathbf{k}\downarrow} (1 - t \cos 4\phi_h) (U \sin^2 \phi_h + J \cos^2 \phi_h) e_{Y-\mathbf{p}\downarrow} e_{Y\mathbf{p}\downarrow} \cos^2 \phi_Y + h.c. \quad (S12)$$

Instead of deriving how the angular dependence of the hole gap arises due to SOC or renormalization, we introduce a phenomenological parameter $-t \cos 4\theta_h$ in the pairing interaction to account for the angular dependence of the SC gap on h even in the tetragonal phase. Note that the C_4 symmetry is still conserved in the presence of this term. In our numerical calculation, we set $t = 0.2 \ll 1$.

Adding them together yields:

$$\begin{aligned} H_{\text{pair}} = & \sum_{\mathbf{k}, \mathbf{p}} h_{\mathbf{k}\uparrow}^\dagger h_{-\mathbf{k}\downarrow}^\dagger (1 - t \cos 4\phi_h) [U_s (e_{X,-\mathbf{p}\downarrow} e_{X,\mathbf{p}\uparrow} \cos^2 \phi_X + e_{Y,-\mathbf{p}\downarrow} e_{Y,\mathbf{p}\uparrow} \cos^2 \phi_Y) \\ & + U_d \cos 2\phi_h (e_{X,-\mathbf{p}\downarrow} e_{X,\mathbf{p}\uparrow} \cos^2 \phi_X - e_{Y,-\mathbf{p}\downarrow} e_{Y,\mathbf{p}\uparrow} \cos^2 \phi_Y)] + h.c. \end{aligned} \quad (S13)$$

with $U_s = U + J$ and $U_d = U - J$. In our calculation, we set $U_d = U_s$. Note that $\cos^2 \phi_{X,Y}$ is the orbital weight of $d_{yz,xz}$ on the $e_{X,Y}$ band and $\cos^2 \phi_h$ ($\sin^2 \phi_h$) are the weights of d_{yz} (d_{xz}) orbitals on the hole band. These weights can be obtained by diagonalization of the matrix $H_{\Gamma,X,Y}$ with the nematic terms.

As shown in the previous sections, $\cos^2 \phi_{X,Y} \approx A_{X,Y}^2 \sin^2 \theta_{X,Y}$ with $A_{X,Y} \approx A(1 \mp \Phi_e)$ if only the first order of the nematic order parameter $\Phi_{h,e}$ is kept in the expansion. Additionally, $\cos 2\phi_h \approx \cos 2\theta_h + \Phi_h \cos 4\theta_h - \Phi_h$. For small nematicity and $t \ll 1$, the $\cos 4\theta_h$ terms can be neglected in the pairing interaction. This gives

$$H_{\text{pair}} = \frac{A^2}{2} \sum_{j=X,Y} h_k^\dagger h_{-k}^\dagger (1 - \cos 2\theta_j) (A_j + B_j \cos 2\theta_h) e_{j,p} e_{j,-p} \quad (\text{S14})$$

$$\text{with } A_{X,Y} = [U_s(1 \mp 2\Phi_e) \mp U_d\Phi_h], \text{ and } B_{X,Y} = [\pm U_d - 2\Phi_e U_d] \quad (\text{S15})$$

III. SOLUTION OF THE GAP EQUATIONS

Starting with the pairing interaction presented in Eq. S13, the linearized gap equation becomes (see Fig. S1)

$$\begin{aligned} \Delta_h(\mathbf{k}_h) = & - (1 - \beta \cos 4\theta_h) \left[(U_s + U_d \cos 2\phi_h) \int \frac{d^2k}{(2\pi)^2} \frac{\tanh(\beta\epsilon_{X,\mathbf{k}}/2)}{2\epsilon_{X,\mathbf{k}}} \cos^2 \phi_X \Delta_X \right. \\ & \left. + (U_s - U_d \cos 2\phi_h) \int \frac{d^2k}{(2\pi)^2} \frac{\tanh(\beta\epsilon_{Y,\mathbf{k}}/2)}{2\epsilon_{Y,\mathbf{k}}} \cos^2 \phi_Y \Delta_Y \right] \end{aligned} \quad (\text{S16})$$

$$\Delta_X(\mathbf{k}_X) = - \cos^2 \phi_X \int \frac{d^2k}{(2\pi)^2} \frac{\tanh(\beta\epsilon_{h,\mathbf{k}}/2)}{2\epsilon_{h,\mathbf{k}}} (1 - \beta \cos 4\phi_h) (U_s + U_d \cos 2\phi_h) \Delta_{h,\mathbf{k}} \quad (\text{S17})$$

$$\Delta_Y(\mathbf{k}_Y) = - \cos^2 \phi_Y \int \frac{d^2k}{(2\pi)^2} \frac{\tanh(\beta\epsilon_{h,\mathbf{k}}/2)}{2\epsilon_{h,\mathbf{k}}} (1 - \beta \cos 4\phi_h) (U_s - U_d \cos 2\phi_h) \Delta_{h,\mathbf{k}} \quad (\text{S18})$$

We numerically solved this equation using the band structure and interaction parameters discussed above and the results are presented in Fig. 2. We found that the gap on the hole pocket is roughly proportional to $1 + 0.65 \cos 2\theta_h - 0.1 \cos 4\theta_h$.

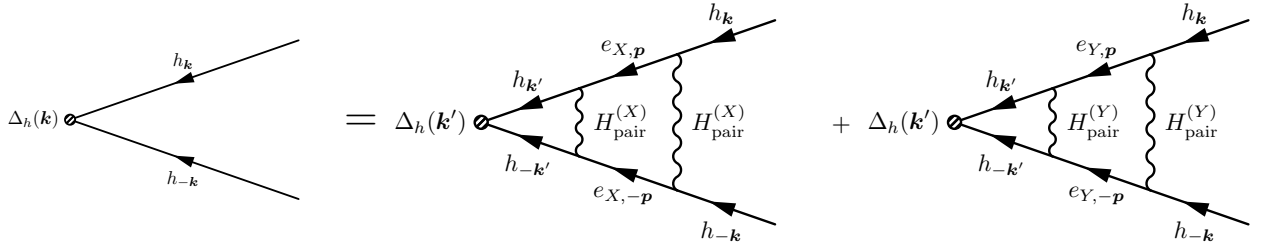


Figure S1. The gap equation for the hole pocket at $T = T_c$, with spin indices suppressed.

We proceed now with the derivation of the analytical expression of the SC gap in leading order in $\Phi_{h,e}$. For this purpose, we start with the approximated pairing interaction in Eq. S14. The pairing equations become

$$\begin{aligned} \Delta_h(\mathbf{k}_h) = & - A^2 \left[(A_X + B_X \cos 2\theta_h) \int \frac{d^2k}{(2\pi)^2} \frac{\tanh(\beta\epsilon_{X,\mathbf{k}}/2)}{2\epsilon_{X,\mathbf{k}}} \sin^2 \theta_X \Delta_X \right. \\ & \left. + (A_Y + B_Y \cos 2\theta_h) \int \frac{d^2k}{(2\pi)^2} \frac{\tanh(\beta\epsilon_{Y,\mathbf{k}}/2)}{2\epsilon_{Y,\mathbf{k}}} \sin^2 \theta_Y \Delta_Y \right] \\ \Delta_X(\mathbf{k}_X) = & - A^2 \sin^2 \theta_X \int \frac{d^2k}{(2\pi)^2} \frac{\tanh(\beta\epsilon_{h,\mathbf{k}}/2)}{2\epsilon_{h,\mathbf{k}}} (A_X + B_X \cos 2\theta_h) \Delta_{h,\mathbf{k}} \\ \Delta_Y(\mathbf{k}_Y) = & - A^2 \sin^2 \theta_Y \int \frac{d^2k}{(2\pi)^2} \frac{\tanh(\beta\epsilon_{h,\mathbf{k}}/2)}{2\epsilon_{h,\mathbf{k}}} (A_Y + B_Y \cos 2\theta_h) \Delta_{h,\mathbf{k}} \end{aligned} \quad (\text{S19})$$

We can then parametrize the gaps as

$$\Delta_h = \Delta_1 + \Delta_2 \cos 2\theta_h, \quad \Delta_X = \Delta_3 \sin^2 \theta_X \text{ and } \Delta_Y = \Delta_4 \sin^2 \theta_Y. \quad (\text{S20})$$

The gap equations for Δ_i can be written in a matrix form. To further simplify the notation, we define

$$\begin{aligned} \Xi_X &= \int \frac{d^2k}{(2\pi)^2} \frac{\tanh(\beta\epsilon_{X,\mathbf{k}}/2)}{2\epsilon_{X,\mathbf{k}}} \sin^4 \theta_X & \Xi_Y &= \int \frac{d^2k}{(2\pi)^2} \frac{\tanh(\beta\epsilon_{Y,\mathbf{k}}/2)}{2\epsilon_{Y,\mathbf{k}}} \sin^4 \theta_Y \\ \Xi_{h,j} &= \int \frac{d^2k}{(2\pi)^2} \frac{\tanh(\beta\epsilon_{h,\mathbf{k}}/2)}{2\epsilon_{h,\mathbf{k}}} (\cos 2\theta_h)^j \quad \text{with } j = 0, 1, 2. \end{aligned} \quad (\text{S21})$$

All these integrals are $O(\ln(\Lambda/T))$, which is given by the band dispersion in the tetragonal phase. In the weak coupling limit, we therefore can keep only the logarithmic term to expand the SC gap to the leading order of nematicity and neglect the change of band dispersion by the nematicity. Therefore, $\epsilon_{e_X}(\theta) = \epsilon_{e_Y}$ and ϵ_h is still C_4 symmetric, leading to $\Xi_X = \Xi_Y = \Xi_e$ and $\Xi_{h,1} = 0$. Furthermore, with quadratic hole dispersion, $\Xi_{h,2} = \Xi_{h,0}/2$. $\Xi_{h,0} = \Pi_h$ is the usual particle-particle bubble for the hole pocket. The matrix equations for Δ_j becomes

$$\begin{pmatrix} \Delta_1 \\ \Delta_2 \end{pmatrix} = -A^2 \Xi_e \begin{pmatrix} A_X & A_Y \\ B_X & B_Y \end{pmatrix} \begin{pmatrix} \Delta_3 \\ \Delta_4 \end{pmatrix}, \quad \begin{pmatrix} \Delta_3 \\ \Delta_4 \end{pmatrix} = -A^2 \Pi_h \begin{pmatrix} A_X & B_X/2 \\ A_Y & B_Y/2 \end{pmatrix} \begin{pmatrix} \Delta_1 \\ \Delta_2 \end{pmatrix} \quad (\text{S22})$$

To solve this equation, we write

$$\begin{pmatrix} \Delta_1 \\ \Delta_2 \end{pmatrix} = A^4 \Xi_e \Pi_h \begin{pmatrix} A_X & A_Y \\ B_X & B_Y \end{pmatrix} \begin{pmatrix} A_X & B_X/2 \\ A_Y & B_Y/2 \end{pmatrix} \begin{pmatrix} \Delta_1 \\ \Delta_2 \end{pmatrix} = (M_0 + M_1) \begin{pmatrix} \Delta_1 \\ \Delta_2 \end{pmatrix}, \quad (\text{S23})$$

where the matrix M_0 contains no nematic terms, and $M_1 \sim O(\Phi_{h,e})$. With the expression of $A_{X,Y}$ and $B_{X,Y}$ in Eq. S15, we find

$$M_0 = 2A^4 \Xi_e \Pi_h \begin{pmatrix} U_s^2 & 0 \\ 0 & U_d^2/2 \end{pmatrix}, \quad M_1 = -A^4 \Xi_e \Pi_h (2U_d^2 \Phi_h + 8U_s U_d \Phi_e) \begin{pmatrix} 0 & 1/2 \\ 1 & 0 \end{pmatrix} \quad (\text{S24})$$

We see Δ_1 and Δ_2 decouples in M_0 , reflecting that s - and d -wave are two pairing instabilities. When $U_s > U_d$, s -wave is the leading solution, with T_c given by the equation $2A^4 U_s^2 \Xi_e \Pi_h = 1$. s -wave and d -wave are mixed due to the perturbative term M_1 . To leading order in M_1 , the solution is given by

$$\alpha = \frac{\Delta_2}{\Delta_1} \approx -\frac{U_s U_d}{U_s^2 - U_d^2/2} \left(4\Phi_e + \frac{U_d}{U_s} \Phi_h \right). \quad (\text{S25})$$

As discussed before, we set $\Phi_e \sim -0.1$, $\Phi_h = 0.2$, and $U_d/U_s = 1$, leading to $\alpha \approx 0.4$. This value is almost half of our numerical results by solving Eqs. S16–S18.

For the electron pockets, we find:

$$\Delta_{e_X} = -A^2 \sin^2 \theta_X \Pi_h \left(A_X \Delta_1 + \frac{B_X}{2} \Delta_2 \right) \approx -A^2 \Pi_h \sin^2 \theta_X U_s \Delta_1 \left[1 - 2\Phi_e - \frac{U_d}{U_s} \left(\Phi_h - \frac{\alpha}{2} \right) \right] \quad (\text{S26})$$

$$\Delta_{e_Y} = -A^2 \sin^2 \theta_Y \Pi_h \left(A_Y \Delta_1 + \frac{B_Y}{2} \Delta_2 \right) \approx -A^2 \Pi_h \sin^2 \theta_Y U_s \Delta_1 \left[1 + 2\Phi_e + \frac{U_d}{U_s} \left(\Phi_h - \frac{\alpha}{2} \right) \right] \quad (\text{S27})$$